





## Open Archive Toulouse Archive Ouverte (OATAO)

OATAO is an open access repository that collects the work of Toulouse researchers and makes it freely available over the web where possible

This is an author's version published in: <http://oatao.univ-toulouse.fr/24441>

Official URL: <https://doi.org/10.1111/jace.12559>

### To cite this version:

Aguilar-Arias, Jaime and Hotza, Dachamir and Lenormand, Pascal  and Ansart, Florence  *Planar Solid Oxide Fuel Cells Using PSZ, Processed by Sequential Aqueous Tape Casting and Constrained Sintering*. (2013) *Journal of the American Ceramic Society*, 96 (10). 3075-3083. ISSN 0002-7820

Any correspondence concerning this service should be sent to the repository administrator: [tech-oatao@listes-diff.inp-toulouse.fr](mailto:tech-oatao@listes-diff.inp-toulouse.fr)

# Planar Solid Oxide Fuel Cells Using PSZ, Processed by Sequential Aqueous Tape Casting and Constrained Sintering

Jaime Aguilar-Arias,<sup>‡,§,†</sup> Dachamir Hotza,<sup>‡</sup> Pascal Lenormand,<sup>¶</sup> and Florence Ansart<sup>¶</sup>

<sup>‡</sup>Núcleo de Pesquisa em Materiais Cerâmicos, CERMAT, Universidade Federal de Santa Catarina UFSC, CEP: 88040 900, Florianópolis, Brazil

<sup>§</sup>Grupo de Procesos Químicos y Biológicos, Universidad Nacional de Colombia UNAL, CP 111321, Bogotá, Colombia

<sup>¶</sup>Institut Carnot CIRIMAT UMR CNRS 5085, 31062 Toulouse, Cedex 9, France

**A process for obtaining planar anode-supported solid oxide fuel cells was developed. Aqueous-based slurries were prepared and sequentially deposited via tape casting to form half cell tapes consisting of the electrolyte, functional, and structural anode. Sintering of the three-layered tapes was done in two stages: presintering circular samples of 25 mm diameter in free conditions first, and then sintering them using zirconium disks as light loads (90 Pa), to obtain half cells having 20 mm and 3.8 m<sup>-1</sup> in diameter and curvature, respectively. Active materials for the electrolyte, anode, and cathode were partially stabilized zirconia (PSZ), Ni and LSM, respectively. Finally, thicknesses of complete cells were 400, 30, 30, and 80 μm for the structural anode, functional anode, electrolyte, and cathode, respectively. The cells were tested in a no-chamber (direct-flame) setup evaluating electrochemical performance and shock thermal resistance. Open circuit voltage was 830 mV at 560°C using methanol as fuel in a burner with porous media to modify the shape of the flame. Cells were also strong enough to resist the rapid temperature changes during several no-chamber tests.**

## I. Introduction

SOLID oxide fuel cells (SOFC) are electrochemical devices that convert the chemical energy available in fuels directly into electricity. As the mechanism of this conversion is not through shaft work, they are not limited by the second law of thermodynamics, so that these devices exhibit greater efficiencies than those of the internal combustion engines. SOFC configuration can be tubular or planar, with the planar having some advantages for stacking and industrial production.<sup>1</sup> Most used electrolyte material is zirconium oxide in its cubic phase, but for pure ZrO<sub>2</sub> this phase is only stable above 2300°C, while addition of 8 mol% yttrium oxide (Y<sub>2</sub>O<sub>3</sub>) forms a stable mixture with cubic crystalline phase at about 1000°C,<sup>2</sup> so called yttria stabilized zirconia (YSZ).

Partially stabilized zirconia (PSZ) is the name given to YSZ when the amount of yttrium is not sufficient to form only the cubic phase, presenting instead a mixture of meta stable tetragonal, cubic, and monoclinic phases of zirconium oxide. PSZ mechanical properties make it useful for several applications,<sup>3</sup> and its use in fuel cells is under study.<sup>4,5</sup> PSZ is commonly prepared by mixing known quantities of zirconium oxide and yttrium oxide at high temperatures, and then

cooled rapidly to obtain the metastable phases. The final composition of the phases depends on the thermal history of the material, in agreement with the phase diagram for the yttria zirconia system.<sup>2</sup>

One concern that may arise about the use of PSZ as component in SOFC is the microstructure degradation due to the martensitic transformation of the intergranular tetragonal to monoclinic phase, causing failure by cracking of the material, as observed at temperatures around 300°C in the presence of humidity.<sup>6</sup> However, at SOFC operating temperatures this problem seems to be less deleterious, as PSZ is effectively used as porous substrate for the anode in so called integrated planar solid oxide fuel cells (IP SOFC), which have been developed since the 90 s.<sup>7</sup> The use of PSZ is reported in the literature as an adequate material for the porous substrate in IP SOFC.<sup>8–10</sup> In this design, individual (interconnected) SOFC cells are attached by the anode to the surfaces of planar porous plates that can be made of PSZ, having wafered channels so that the humidified fuel flows through the channels and percolate through the porous media into the anode, as well as the products leaving the anode.

A versatile process for producing planar SOFCs is tape casting of slurries prepared with organic solvents and powders of the components of the cell, which are applied over a smooth surface and dried to obtain thin tapes. These tapes are often laminated to obtain the green cell, and functional layers are usually screen printed on the support after sintering. Cofiring half cells (electrolyte and anode) and finally application and sinter of the cathode is a reliable method to obtain planar cells, but the processing technique must avoid common problems such as delamination and camber.

Solvent free processing has received special attention in the recent years for health and environmental aspects.<sup>11,12</sup> In a previous work, components were selected for processing the fuel cells, and formulations were optimized for obtaining water based slurries to be used for tape casting processing.<sup>13</sup>

Cologna *et al.*<sup>14</sup> studied the sintering of bi layered planar SOFC obtained by sequential aqueous tape casting. The samples were 280 μm thick, and 2 cm<sup>2</sup> active area. They show that camber during sintering is determined by the particle size of the YSZ powders used both in the electrolyte and the anode. Testing two kinds of powders, a fine ( $d_{50}$  = 0.3 μm) and a coarse ( $d_{50}$  = 0.7 μm), the best results obtained were for fine powder both in the electrolyte and the anode, and for coarse powder in the electrolyte and a mixture of fine (50 wt%) and coarse powders in the anode. For other combinations, the results yield in curved samples both upward and downward.

Another method to obtain planar fuel cells is the use of loads during, or after sintering the half cells.<sup>15–18</sup> Lee *et al.*<sup>16</sup> applied load during sintering, using ceramic arches, which

M. Menon—contributing editor

Author to whom correspondence should be addressed. e-mail: jlaguilara@unal.edu.co

are placed around the cell to support the load in the beginning of the process, but that while heating, become planar, letting the load act gradually over the cell. Mücke *et al.*<sup>17</sup> and Fischer *et al.*<sup>15</sup> indicated that flattening can be done after sintering, using a special furnace.

The purpose of this work was to obtain planar SOFC but ton cells by tape casting, applying aqueous slurries directly on the predried tapes (sequential tape casting). Anode supported cells are to be obtained, so three kinds of slurries were applied, including the structural anode, functional anode, and the electrolyte. These goals of course are in addition to the electrolyte densification and gas tightness. A comparison of the traditional and proposed processing techniques is presented in Table I.

Sequential tape casting requires special attention to avoid problems occurring, like rides, mixing, and cracking during drying the slurries. Rieu *et al.*<sup>19</sup> showed the importance of carefully controlling the drying conditions of the tapes, temperature, flow, and composition of environment to control the rate of evaporation, especially when using organic solvents.

In theory, the curvature in sintered multilayered structures could be estimated, as it depends on the thicknesses, viscosities, and sintering shrinkage of the layers. The normalized degree of curvature ( $k$ ) for a bilayer structure is expressed as follows: (Evans and Hutchinson,<sup>20</sup> Cai *et al.*<sup>21</sup>)

$$k = \frac{h_1 + h_2}{R} = \left[ \frac{6(m+1)^2 mn}{m^4 n^2 + 2mn(2m^2 + 3m + 2) + 1} \right] (\varepsilon_2 \quad \varepsilon_1) \quad (1)$$

where  $R$  is the radius of curvature,  $m = \frac{h_1}{h_2}$  and  $n = \frac{\eta_1/(1-\nu_1)}{\eta_2/(1-\nu_2)}$ ,  $h_i$ ,  $\varepsilon_i$ ,  $\eta_i$ , and  $\nu_i$  are, respectively, the thickness, strain, viscosity, and Poisson's ratio for each layer.

With this expression, the nominal mismatch stress ( $\sigma_e = E_1(\varepsilon_2 \quad \varepsilon_1)$ ) can be calculated by measuring the curvature of the samples. For a thin layer over a thick support, as in the case of the half cells,  $m \ll 1$ , Eq. (1) becomes:

$$k = \frac{6mn}{4mn + 1} (\varepsilon_2 \quad \varepsilon_1) \quad (2)$$

Thus, for bi layered half cells (electrolyte functional anode), the mismatch stress is about the residual stress.<sup>20</sup> This is an approximate expression useful only for bi layered structures, that could be useful for predicting curvature of the samples after sintering, but for three layered structures as

those considered in this work, models have not been developed yet.

## II. Experimental Procedure

### (1) Materials

Commercial powders were used to prepare the slurries, for the electrolyte, PSZ (464228; Aldrich, Saint Louis, MO), and for the anode, nickel (II) oxide (NiO) (399523; Aldrich). Chemical composition of the zirconia powder was determined by X Ray Fluorescence (MagixPro PW 2440; Philips, The Netherlands), using the software IQ + 3.0k (Philips, Almelo, The Netherlands) for quantification. Particle size distribution of these powders was determined using a Malvern Z nanosizer (Zen 3600; Malvern Instruments, Malvern, UK), and crystalline phases were determined by X ray diffraction (D4 Endeavor, Bruker AXS; Karlsruhe, Germany).

The compositions of the slurries corresponding to each cell component are presented in Table II. Water based slurries were obtained by ball milling the powders in water for 16 h using ammonium polymethacrylate (Darvan CN; Vanderbilt, Norwalk, CT) as dispersant. After dispersing the powder, the acrylic binder (Mowilith LDM 6138; Clariant, São Paulo, Brazil) and fatty acid diethanolamine (Cocamide DEA; Stepan, Vespasiano, Brazil) were mixed for 30 min, and the slurry was let to settle for 6 h to remove the excess of bubbles.

Figure 1(a) shows the automatic film applicator (1133N; Sheen Instruments, Cambridge, UK) used to apply the slurries. The displaceable bar side moves to the right at a constant velocity adjusted by the speed control. In this figure, a sample of the silicone coated polyester film can be seen (PET SRF 121; HiFi Industrial Film Ltd, Stevenage, UK). The film was used as substrate, and remained fixed during the spreading of the slurry. The moving bar pushes the doctor blade with adjustable micrometer and trapezoidal geometry (1117; Sheen Instruments, UK) shown in Fig. 1(b). Enough volume of the slurry is placed along the blade, depending on the thickness and desired area of the tape, so that it is spread when the bar pushes the doctor blade, and letting to apply carefully several layers without damaging the previous ones. The speed of the doctor blade was set to 50 mm/s. Drying of the samples was carried out at ambient conditions.

To know the temperature at which organics in the tapes are to be removed, analyses were done in a thermo gravimetric analyzer (TGA 2050; TA Instruments, New Castle, DE) following the program: 30°C, 1°C/min, 400°C, 5°C/min, 800°C. For sintering studies, dilatometric test of the structural anode was performed in a TMA/Dilatometer (S60/58648; SETA RAM Instrumentation, Caluire, France) following the program 30°C, 1°C/min, 400°C, 5°C/min, 1500°C.

### (2) Bi-Layered Half-Cell Tape Processing

As a first approach for obtaining planar half cell samples, tapes were prepared having an electrolyte layer followed by a single layer of (functional) anode. As mentioned before, the tape casting equipment allows the direct application of the anode slurry over the predried electrolyte layer. For the electrolyte, a layer with a thickness of 40  $\mu\text{m}$  it was previously set, expecting to obtain a thickness of about 30  $\mu\text{m}$  after sintering. The final doctor blade gap (DBG) was 1250  $\mu\text{m}$ , which lead to obtain dry tapes of about 400  $\mu\text{m}$ .

### (3) Tri-Layered Half-Cell Tape Processing

Structural anode is essentially the same composition as the functional anode (Table II), but with higher porosity, created by a sacrificial component during sintering, commercial corn starch in this case. The sequential tape casting for the tri layered half cells consisted in applying the electrolyte and functional anode in thin layers, and then a thicker layer of structural anode. The slurries were applied in intervals of

**Table I. Comparison of Conventional and Proposed SOFC Processing Techniques**

Parameter	Conventional processing	This work
Tape casting	Individual	Sequential electrolyte anode
Solvent	Organic	Water
Thermopressing	Laminating sheets of electrolyte anode	N/A
Presintering temperature (°C)	N/A	1050
Sintering temperature (°C)	1400	1450
Load on sintering (Pa)	0	90
Load after sintering (Pa)	400 2000	0
Cathode forming	Screen printing	Painting

Table II. Slurries Composition for the Electrolyte, Functional, and Structural Anode

Function	Substance	Cell component (wt%)		
		Electrolyte	Functional anode	Structural anode
Electrolyte	PSZ	55.0	22.0	18.0
Anode	NiO	0.0	33.0	27.0
Pore former	Starch	0.0	0.0	10.0
Binder	Acrylic ester	25.0	25.0	25.0
Dispersant	Ammonium polymethacrylate	1.0	1.0	1.0
Surfactant	Fatty acid DEA	2.5	2.5	2.5
Solvent	Water	16.5	16.5	16.5



(a)



(b)

Fig. 1. Automatic film applicator (a) and doctor blade (b) used to obtain bi and tri layered tapes.

about 30 min, so that the tapes were not completely dried. As in the case of bi layered tape, the final DBG was also 1250  $\mu\text{m}$ , which led to obtain dry tapes of about 400  $\mu\text{m}$ .

#### (4) Sintering

Tape samples were cut in circles of different diameters ranging from 14 to 26 mm, and sintered with the electrolyte facing up in a high temperature furnace (VF1; Vecstar Furnaces, Chesterfield, UK). The sintering program in the furnace was: 1°C/min, 450°C 1 h, 3°C/min, 1450°C 3 h, 5°C/min, 25°C.

Before applying loads, it was necessary to remove the organics and presinter samples to obtain enough mechanical strength to hold the loads without breaking them. A low weight was also desired, so that the sample does not need a high strength, in other words, it was necessary to find a balance between the weight of the load and the presintering temperature. In this way, the densification process was carried out simultaneously with the flattening treatment, allowing particles to accommodate, reducing the residual stresses.

Porosity of the half cells was determined by the ASTM C373<sup>22</sup> method. This method consists in the submersion of the porous samples in boiling water for 5 h. After cooling,

the weights of the wet and dry samples were compared to determine the weight (volume) of water absorbed. The total volume of the sample was obtained by Archimedes, so that the volume fraction could be estimated. An advantage of this method is to determine the open porosity, so that the result gives also an idea of the percolation in the porous media.

Curvature ( $R^{-1}$ ) was used as variable for measuring and determining the effectiveness of the process for obtaining flat samples. Data from other authors were converted into this variable for comparison purposes.

To estimate the curvature, the expression found in ASTM B106 08<sup>23</sup> was used:

$$\frac{1}{R} = \frac{8(d - T)}{D^2 + 4(d - T)T + 4(d - T)^2} \quad (3)$$

where  $D$  is the diameter,  $T$  is the thickness, and  $d$  is the deflection of the sample, as shown in Fig. 2.

Microstructures of the sintered samples were characterized by Scanning Electron Microscopy (SEM) using JEOL Microscopes (JSM6400, and JSM6390LV; JEOL, Tokyo, Japan).

#### (5) Cells Finishing

A mixture of powders having 60 wt% lanthanum strontium manganite,  $\text{La}_{0.8}\text{Sr}_{0.2}\text{MnO}_3$ , LSM 20 (704296; Aldrich) and 40 wt% PSZ (464228; Aldrich) was used to prepare the slurry for the cathode. The slurry was prepared using the same procedure as described for the electrolyte and anode slurries, and was applied by directly painting it on the electrolyte, leaving about 2 mm in the border unpainted. The active area of the cells was 1.8  $\text{cm}^2$ .

After painting, the complete cell was sintered using the following program: 1°C/min, 450°C 1 h, 3°C/min, 1100°C 3 h, 5°C/min. The direct application of LSM cathode directly on the electrolyte was not ideal, because of the known reaction between  $\text{ZrO}_2$  and LSM to form phases such as  $\text{La}_2\text{Zr}_2\text{O}_7$ .<sup>24,25</sup> Nevertheless, for simplicity in processing studies like here, these reactions can be tolerable at some extent considering the acceptable results found in literature working in this way.<sup>18,26,27</sup> The reason to follow this processing

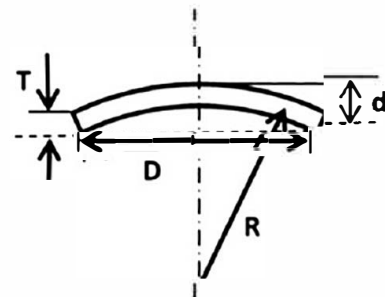


Fig. 2. Variables for calculating curvature according to ASTM B106.



sequence was the lack of the equipment necessary to deposit a very thin layer of a ceria based electrolyte before the cathode application. Some measures were also taken, trying to lower the reaction kinetics, such as using the lower possible sintering temperature time (ensuring cathode adhesion), and the 60/40 proportion in LSM/PSZ.<sup>25</sup>

### (6) Electrochemical Testing

Electrochemical characterization of the cells was performed in an 855 Fuel Cell Test System (855 SOFC Test; Scribner Associates Inc., Southern Pines, NC), in a no chamber setup. The test consists in operating the cell using a flame of a burning fuel as source both of heat and fuel.<sup>28</sup> In Fig. 3, it is shown a sketch of the setup used. In this design, a porous media is used to stabilize the flame and to improve the efficiency of the combustion by preheating the fuel.<sup>29,30</sup> The liquid fuel (methanol) enters as liquid from the bottom, being heated and vaporized inside, and burns over the surface of the porous media. The flame surrounds the bottom of the cell facing the anode, so that contact is favored with the inner region of the flame, which is rich in hydrogen and carbon monoxide that are used as fuel for the cell.<sup>31</sup> The top part is open to atmosphere, so that the cathode has a source of oxygen in the air.<sup>32</sup>

The temperature was measured using a thermocouple (type *K*) placed in contact to the surface of the anode in the center of the cell, as depicted in Fig. 3. Temperature gradients are expected to occur, but they were difficult to measure. It is expected, for instance, that in the outer region close to the border of the anode the temperature was higher, as it was the place for the exothermic reactions to happen, but at the same time in this region there is almost neither H<sub>2</sub> nor CO, for the cell to convert and increase the current density.<sup>28</sup> In these terms, the center of the cell is a representative location for measuring the temperature. Other consideration about temperature was that during the electrochemical tests it was not set to some target, but it was rather measured in the most stable conditions obtained in the available experimental setup.

## III. Results and Discussion

### (1) Zirconia Powder Characterization

Chemical composition of the zirconia powder is presented in Table III. Molar composition of yttrium oxide is about 5%, which corresponds to, PSZ.<sup>2</sup> Particle size for the zirconia powder was found to be  $d_{50}$  0.47  $\mu\text{m}$  ( $d_{10}$  0.26  $\mu\text{m}$ ,  $d_{90}$  0.85  $\mu\text{m}$ ). Analysis by X ray diffraction for zirconia powder (Fig. 4) shows a mixture containing mainly cubic (PDF: 00 030 1468) and tetragonal phases (00 048 0224) and a small amount of monoclinic phase (PDF: 01 070 2491), as expected for PSZ. The cubic phase is the ionic conducting phase, so the presence of the tetragonal phase reduces the conductivity, but also improves the mechanical strength of the material, so it was interesting to test the performance of the cell with this material.

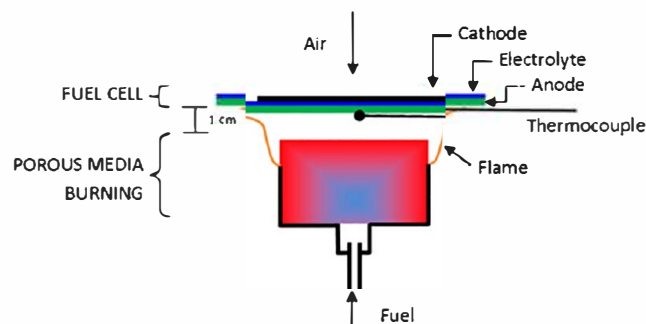


Fig. 3. No chamber setup for testing solid oxide fuel cells.

Table III. Chemical Composition of PSZ by X-Ray Fluorescence

Compound/Element	Composition	
	(wt%)	(mol%)
ZrO <sub>2</sub>	88.48	92.28
Y <sub>2</sub> O <sub>3</sub>	8.83	5.03
HfO <sub>2</sub>	1.98	1.21
MgO	0.18	0.57
Tl	0.18	0.11
La	0.15	0.14
S	0.14	0.57
As	0.06	0.10

### (2) NiO Powder Characterization

Particle size distribution for NiO was  $d_{50}$  1.34  $\mu\text{m}$  ( $d_{10}$  1.08  $\mu\text{m}$ ,  $d_{90}$  1.72  $\mu\text{m}$ ), which is about three times the size of the YSZ, and adequate for the anode performance, as suggested in the literature<sup>33,34</sup>. XRD analysis of the powder shown in Fig. 5 indicates that is entirely composed by NiO as bunsenite cubic phase (PDF: 01 071 1179).

### (3) Anode and Electrolyte Tapes Characterization

Results from thermogravimetric analyses are shown in Fig. 6. As it can be seen, organics removal begins at about 250°C and finishes at about 500°C for the electrolyte and about 400°C for the anode. Accordingly, the heating rate must be slow until about 450°C, after that, heating rate can be increased.

Results of dilatometric test of the structural anode are shown in Fig. 7 for the specific shrinkage (a) and shrinking rate (b) that organics removal creates an initial expansion and that the sintering begins at about 1000°C with maximum shrinking rate at 1250°C [Fig. 5(b)], with a total shrinkage of 23%.

### (4) Bi-Layered Half-Cell Processing

Tapes were cut in circular samples having 26 mm diameter and sintered based on the results of TGA and dilatometric analyses. The sintered samples had an average diameter of 16.7 mm, which represent a shrinkage of about 24% in agreement with the dilatometric results. Some camber was observed, but there were no other problems such as delaminating or cracks.

The curvature for the sintered samples and its uncertainty were calculated based on the Eq. (3), results are shown in Table IV. Uncertainty for the curvature was calculated according to the law of propagation of uncertainty.<sup>35</sup> The reported value in the table is that of the combined uncertainty, so for a confidence level of 68%, the value of curvature is  $31 \pm 7 \text{ m}^{-1}$ .

In Fig. 8, the SEM images are shown for the bi-layered half cell, as well as the respective chemical analysis. It can be seen that the electrolyte is well defined with a thickness of about 20  $\mu\text{m}$ , showing good densification, whereas the anode shows good distribution of the PSZ and the NiO, and porosity.

### (5) Tri-Layered Half-Cell Processing

An image of one of the tapes obtained by sequential tape casting is presented in Fig. 9. It was possible to process tapes with area over 100 cm<sup>2</sup>.

### (6) Sintering without Loads

For the first tests, no load was applied for sintering, and the tri-layered tapes were cut in circular samples having four

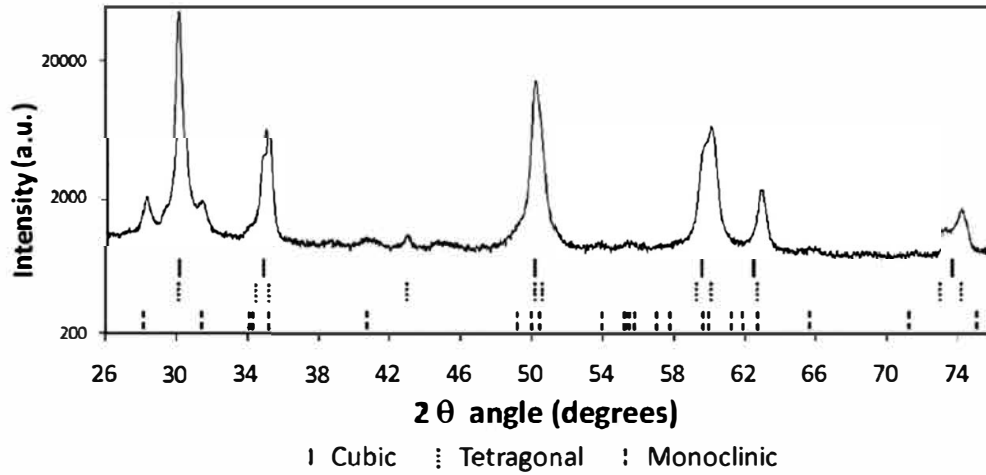


Fig. 4. XRD pattern of partially stabilized zirconia powder.

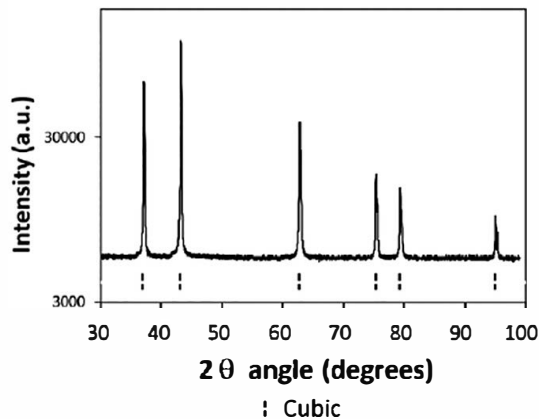


Fig. 5. XRD pattern of the NiO powder.

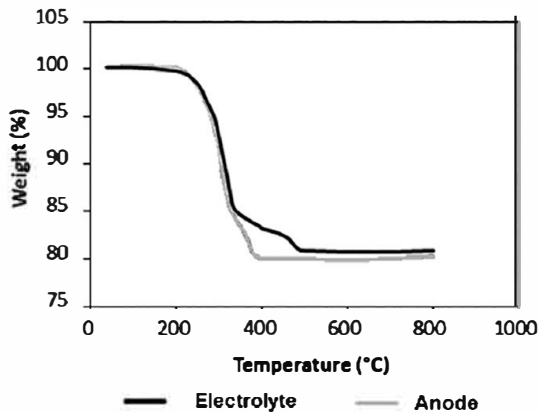


Fig. 6. Thermogravimetric analyses for the tapes of electrolyte and anode.

different diameters (14, 16, 18, and 26 mm) to evaluate the effect of the diameter on the curvature, what is shown in Fig. 10. It may be seen that there is a deleterious effect when cutting samples below 18 mm.

For 26 mm samples, the curvature after sintering is lower than for the bi layered samples, as shown in Table V. In this case, the curvature is  $15 \pm 4 \text{ m}^{-1}$  for a level of confidence of 68%. These results are comparable to those obtained by Park *et al.*,<sup>18</sup> and Cologna *et al.*<sup>14</sup>

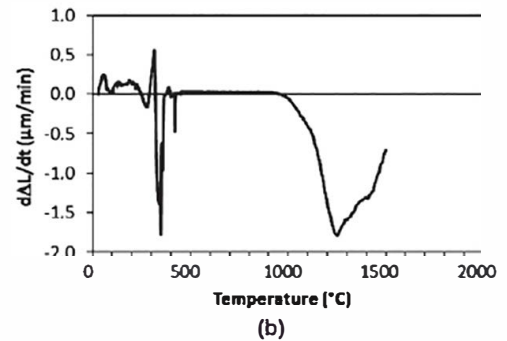
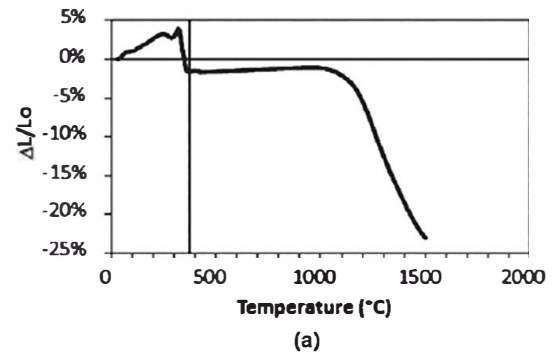


Fig. 7. Dilatometric test for the structural anode: Specific shrinkage (a) and shrinking rate (b).

Table IV. Curvature of the Bi-Layered Half Cells Sintered at 1450°C Without Load

	Diameter ( <i>D</i> , mm)	Thickness ( <i>T</i> , mm)	Deflection ( <i>d</i> , mm)	Curvature ( $1/R$ , $\text{m}^{-1}$ )
Average	18.198	0.419	1.889	31.7
Uncertainty	0.464	0.022	0.223	5.7

#### (7) Constrained Sintering Using Loads

After several tests, it was found adequate to presinter the samples up to 1050°C, followed by sintering up to 1450°C using YSZ disks (4.9 g) as load for flattening treatment, equivalent to 90 Pa, considering samples having 26 mm diameter. This is considered a low charge, compared to the values reported by Park *et al.*,<sup>18</sup> being in the range 460 1700 Pa. The sintering profile and some of the half cells obtained are shown in Fig. 11.

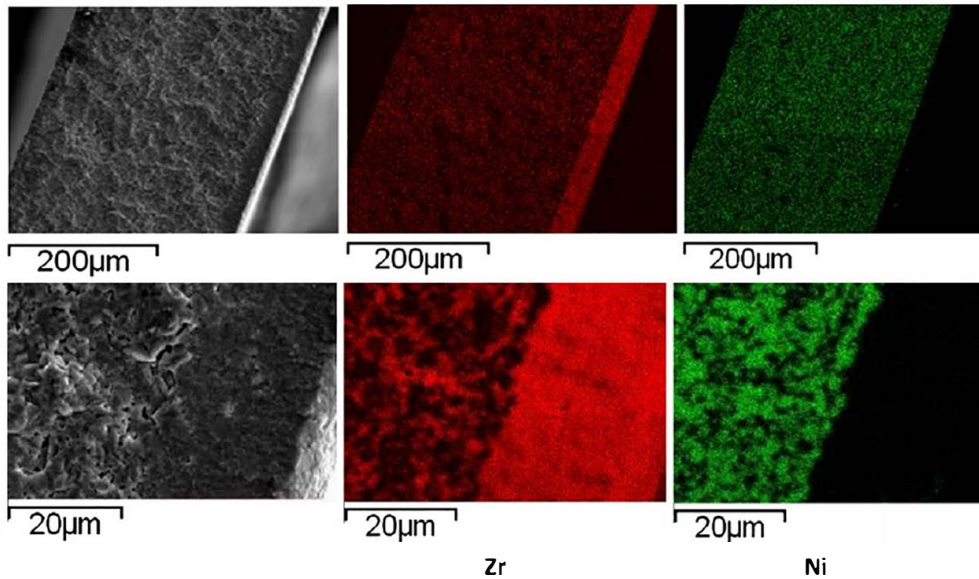


Fig. 8. SEM images with chemical analysis for Zr and Ni for the bi-layered half cell.



Fig. 9. Tape obtained by sequential tape casting, showing electrolyte, functional, and structural anode layers.

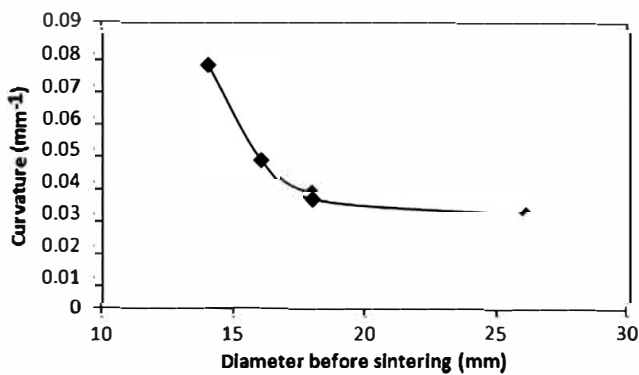
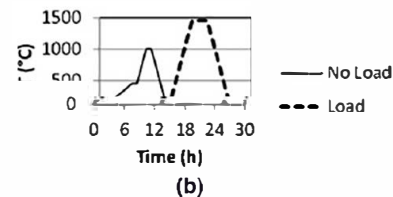


Fig. 10. Curvature of the sintered samples without load having initial thickness of 400 µm.



(a)



(b)

Fig. 11. Sintering in two stages using yttria stabilized zirconia disk load in the second stage. (a) Samples obtained, (b) Sintering profile.

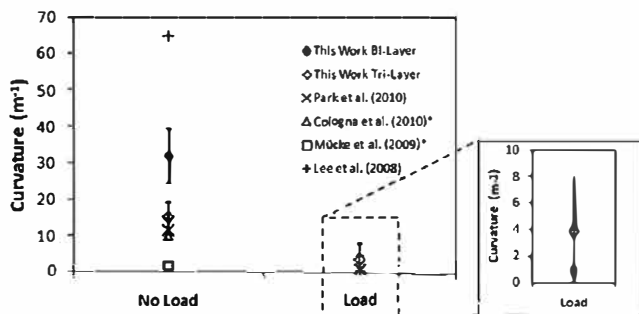
Table V. Curvature of the Tri-Layered Half Cells Sintered Without Load at 1450°C

	Diameter (D, mm)	Thickness (T, mm)	Deflection (d, mm)	Curvature (1/R, m <sup>-1</sup> )
Average	19.724	0.578	1.413	15.3
Uncertainty	0.129	0.036	0.181	3.8

Table VI. Curvature of the Cells Sintered at 1450°C Using Load

	Diameter (D, mm)	Thickness (T, mm)	Deflection (d, mm)	Curvature (1/R, m <sup>-1</sup> )
Average	20.018	0.396	0.602	3.8
Uncertainty	0.281	0.078	0.171	3.8





\* These works don't report the use of loads.

Fig. 12. Effect of the use of loads on the curvature of the half cells.

of Mücke *et al.*,<sup>17</sup> shows the best results without loads, but has the drawback of being at a very low heating rate. A flat tening treatment using loads after sintering is also reported, resulting in extended heat treatments.

Figure 13 shows the SEM images of the surface of the electrolyte. It may be seen that there are no cracks and a grain size of about 300 nm.

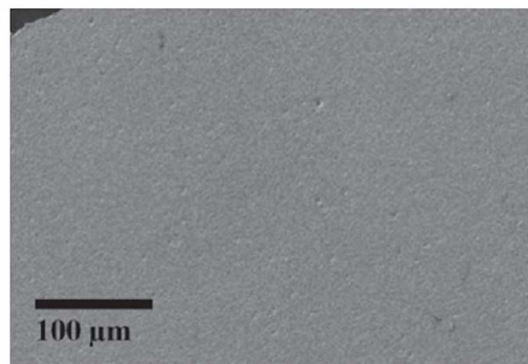
The XRD of the same surface in Fig. 14 shows evidence for the cubic (PDF: 00 030 1468) and the tetragonal (PDF: 00 048 0224) phases, in contrast to the XRD of the powder (Fig. 4), where there was evidence of monoclinic phase. Furthermore, the peaks for cubic and tetragonal phases are enhanced, indicating also an increase in crystallinity. Srivastava *et al.*<sup>36</sup> showed that XRD is useful to differentiate the cubic and tetragonal phases for PSZ because there is a splitting of the peaks for cubic phase into two peaks for the tetragonal phase, as may be seen in the angles 34° 35°, 59° 60°, and 73° 75°. Another feature is the absence of peaks of NiO, indicating that there was no contamination or mixing of the anode to the electrolyte layers.

SEM image for the cross section of the tri layered half cell in Fig. 15 shows the porosity gradient desired for the structural and the functional anode, as well as the densification and thinness of the electrolyte.

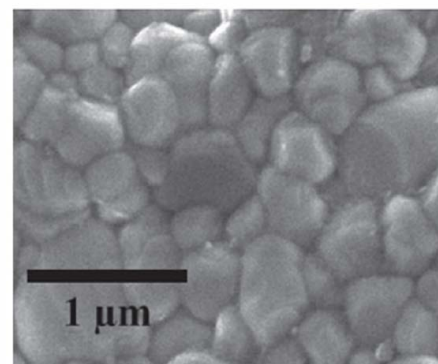
Porosity of the half cells determined by the ASTM C373<sup>22</sup> method, was found to be 38%, which is adequate for SOFC applications, considering the method is for determining open porosity.

#### (8) Cell Finishing

The SEM Image of the complete cell is shown in Fig. 16. An adequate adhesion of the cathode to the electrolyte was obtained. After the anode reduction, the porosity was 47% both for the samples with and without flattening treatment,



(a)



(b)

Fig. 13. SEM images of the half cell facing the electrolyte (a) surface, (b) grain detail.

indicating that the treatment does not affect the porosity. These results are also in agreement with literature reports of increasing porosity in about 10% after anode reduction<sup>33</sup>.

#### (9) Electrochemical Characterization

Figure 17 shows the cell potential for a 50 min test at 560°C when applied different electronic loads during electrochemical characterization. This temperature is lower than that reported by Sun *et al.*<sup>37</sup> for a no chamber setup using methanol (~710°C). It may be explained because in their work a free flame was used, whereas in this work a porous media was employed to modify the shape of the flame.

Tests were done for several times showing relative stability for the potential, being more stable when increasing the

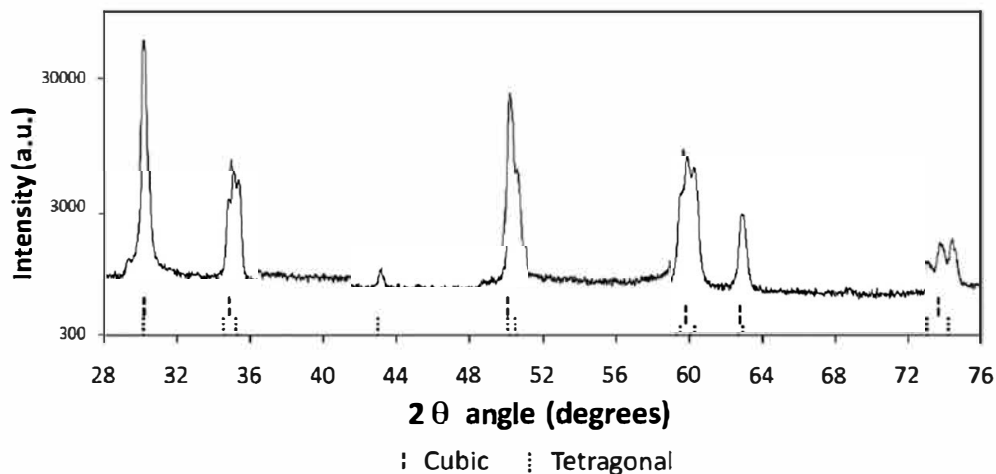


Fig. 14. XRD analyses of the partially stabilized zirconia electrolyte of the sintered half cell.



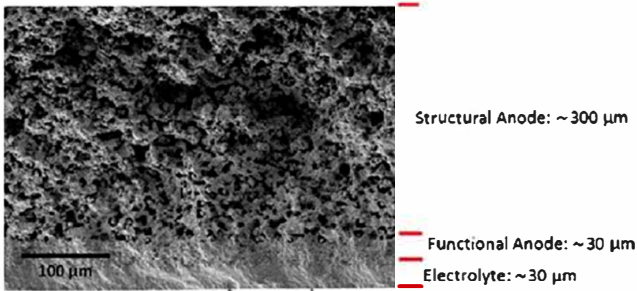


Fig. 15. SEM image of the cross section for the tri layered half cell before reduction.

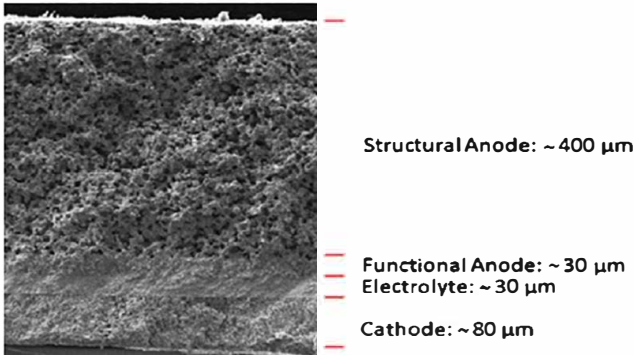


Fig. 16. SEM image of the cross section of the tri layered complete cell.

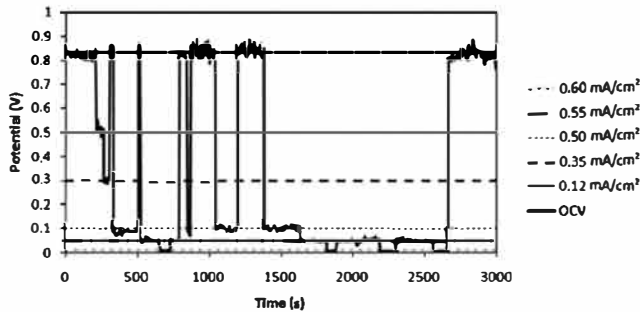


Fig. 17. Electrochemical test of cell potential as a function of time when applied different electronic loads.

electronic load. With the average data collected from the test shown in Fig. 17, was constructed the polarization curve for the cell, as presented in Fig. 18.

Results show that the activation overpotential of the cell is governing on the ohmic and concentration overpotentials, this can be attributed essentially to the low temperature of operation, not enough for the ionic conductivity of the PSZ to be adequate for the cell operation. Temperature was increased by separating the cell and the burner, but the flame became unstable so that the test was not reproducible. Other tests using cubic YSZ show the same performance,<sup>29</sup> so that this behavior is not attributed to the composition of the electrolyte.

This low electrochemical performance can also be attributed to the low conductivity and catalytic activity of LSM for the cathodic reaction, together with the difficulty for oxygen diffusion associated with the no chamber setup.

Postmortem analysis by SEM showed higher porosity of the cells, especially in the functional anode, and a good adhesion of the cathode to the electrolyte, as shown in Fig. 19.

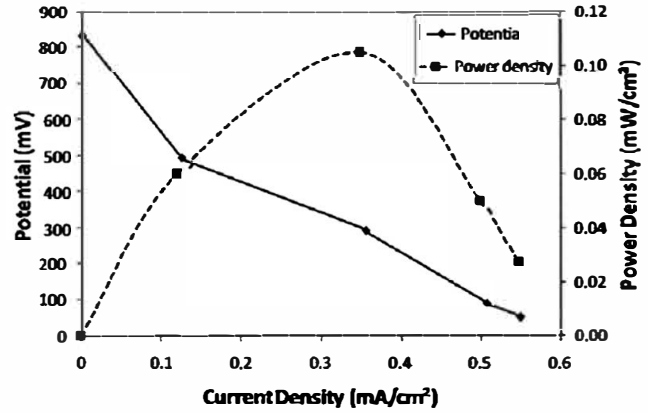


Fig. 18. Electrochemical characterization of the fuel cell.

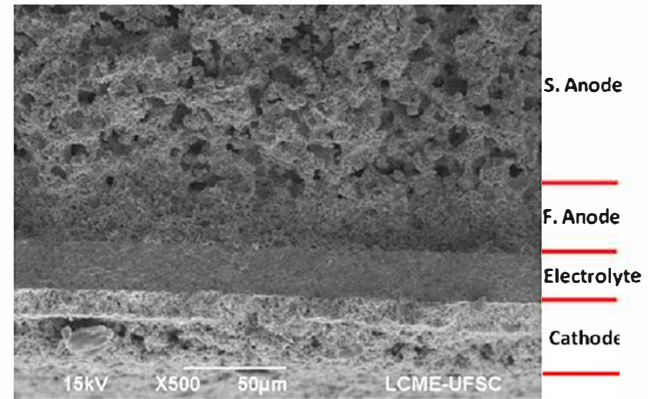


Fig. 19. SEM image of the cell after electrochemical testing.

#### IV. Conclusions

The processing technique using aqueous based slurries and sequential tape casting allow to produce SOFC having a thin, dense electrolyte, and two well distributed and porosity differentiated anodes: a thin one (functional), and a thick one (structural). Applying the electrolyte slurry at first, and sintering samples facing up, allows producing a structure where a thin dense layer is to be well attached to a porous structure.

The flattening treatment using light loads applied on preintered samples (constrained sintering) was successful since in the early stage of the sintering process, the necks formed are enough to support the load, and then, the densification process follow the physical restriction of the planar surfaces in the absence of high stresses. This is in contrast of using loads after full sintering, where the particles were fixed in a certain position, of minimum energy. This would be disturbed by the late flattening treatment, which would require higher loads, creating residual stresses, and affecting the porosity.

The cells effectively resisted the thermal and mechanical stresses during testing. Even in the extreme conditions of thermal shock during the no chamber tests, where temperature changed from room to more than 600°C in less than 1 min, and for several times, there were no failing samples by cracking.

The open circuit voltage obtained, higher than 800 mV, show that PSZ (cubic + tetragonal) has a potential use as SOFC component. The mechanical resistance of the cells produced, makes PSZ an attractive material as alternative for the full cubic YSZ.

Poor electrochemical performance of the cells, may be attributed to the formation of isolating phases in the cath

ode, low ionic conductivity of PSZ, and low electronic conductivity, and catalytic activity of the LSM at the operating temperature, as well as the nature of the no chamber setup for the test.

Obtained results allowed showing that the processing technique is adequate for obtaining SOFC, and that the no chamber setup is an alternative for testing SOFC in laboratory, as a simple, fast, and non destructive test. This same setup is of interest also for Combined Heat and Power applications.

Among the issues to be improved, the more relevant in the scope of this article are those related to increase in the area and current density of the cells. For the area, the limiting step was the availability of wider loads to apply for constrained sintering, but working with larger samples will surely bring other problems, due to the higher failure probability. Thus, requiring to adjust the shrinking rates and presintering temperature, for instance. Regarding the improvement of the current density, there are two fronts: the cell itself, and the no chamber setup for testing. Again, for the scope of this work, it would be desired to try to increase the operating temperature of the cell by modifying the burner, and using the ceria interlayer to avoid the reaction with the cathode in the cell.

### Acknowledgments

Authors acknowledge financial support from CNPq Agency (Brazil), and EULANEST project. Special thanks to the laboratories LabMat UFSC and LCME UFSC for their support.

### References

<sup>1</sup>NETL, National Energy Technology Laboratory. *Fuel Cell Handbook*. 7th edition. US Department of Energy, Morgantown, WV, 2004.

<sup>2</sup>H. G. Scott, "Phase Relationships in the Zirconia-Yttria System," *J. Mater. Sci.*, **10** [9] 1527-35 (1975).

<sup>3</sup>I. Nettleship and R. Stevens, "Tetragonal Zirconia Polycrystal (TZP) A Review," *Int. J. High Technol. Ceram.*, **3** [1] 1-32 (1987).

<sup>4</sup>A. Morales-Rodríguez, A. Bravo-León, A. Domínguez-Rodríguez, and M. Jiménez-Melendo, "High-Temperature Plastic Behavior of TZP Ni Cermet," *J. Am. Ceram. Soc.*, **91** [2] 500-7 (2008).

<sup>5</sup>C. Suci, H. Tikkanen, I. Wærnhus, F. Goga, and E. Dorolti, "Water-Based Tape-Casting of SOFC Composite 3YSZ/8YSZ Electrolytes and Ionic Conductivity of their Pellets," *Ceram. Int.*, **38** [1] 357-65 (2012).

<sup>6</sup>W. Vandermeulen, R. W. Bosch, A. Leenaers, W. Renterghem, and F. Snijkers, "Degradation of 5 mol% Ytria Zirconia by Intergranular Cracking in Water at 300°C," *J. Mater. Sci.*, **45** [20] 5502-11 (2010).

<sup>7</sup>F. J. Gardner, M. J. Day, N. P. Brandon, M. N. Pashley, and M. Cassidy, "SOFC Technology Development at Rolls-Royce," *J. Power Sources*, **86** [1-2] 122-9 (2000).

<sup>8</sup>Y. B. Kim, S. J. Ahn, J. Moon, J. Kim, and H. W. Lee, "Direct-Write Fabrication of Integrated Planar Solid Oxide Fuel Cells," *J. Electroceram.*, **17** [2-4] 683-7 (2006).

<sup>9</sup>K. Oh, J. Kim, S. H. Choi, D. Lee, and J. Moon, "Influence of Reduced Substrate Shunting Current on Cell Performance in Integrated Planar Solid Oxide Fuel Cells," *Ceram. Int.*, **38** [1] 695-700 (2012).

<sup>10</sup>H. Zhu and R. J. Kee, "Two-Dimensional Model of Distributed Charge Transfer and Internal Reforming Within Unit Cells of Segmented-In-Series Solid-Oxide Fuel Cells," *J. Power Sources*, **196** [18] 7654-64 (2011).

<sup>11</sup>D. Hotza and P. Greil, "Review: Aqueous Tape Casting of Ceramic Powders," *Mater. Sci. Eng., A*, **202** [1-2] 206-17 (1995).

<sup>12</sup>R. Sayers, M. Rieu, P. Lenormand, F. Ansart, J. A. Kilner, and S. J. Skinner, "Development of Lanthanum Nickelate as a Cathode for use in Intermediate Temperature Solid Oxide Fuel Cells," *Solid State Ionics*, **192** [1] 531-4 (2011).

<sup>13</sup>V. Moreno, J. Aguilar, and D. Hotza, "8YSZ Tapes Produced by Aqueous Tape Casting," *Mater. Sci. Forum*, **752** 727-8 (2012).

<sup>14</sup>M. Cologna, V. M. Sglavo, and M. Bertoldi, "Sintering and Deformation of Solid Oxide Fuel Cells Produced by Sequential Tape Casting," *Int. J. Appl. Ceram. Technol.*, **7** [6] 803-13 (2010).

<sup>15</sup>W. Fischer, J. Malzbender, G. Blass, and R. W. Steinbrech, "Residual Stresses in Planar Solid Oxide Fuel Cells," *J. Power Sources*, **150**, 73-7 (2005).

<sup>16</sup>S. H. Lee, G. L. Messing, and M. Awano, "Sintering Arches for Cosintering Chamber-Free SOFC Multilayers," *J. Am. Ceram. Soc.*, **91** [2] 421-7 (2008).

<sup>17</sup>R. Mücke, N. H. Menzler, H. P. Buchkremer, and D. Stöver, "Cofiring of Thin Zirconia Films During SOFC Manufacturing," *J. Am. Ceram. Soc.*, **92**, S95-102 (2009).

<sup>18</sup>H. G. Park, H. Moon, S. C. Park, J. J. Lee, D. Yoon, S. -H. Hyun, and D. -H. Kim, "Performance Improvement of Anode-Supported Electrolytes for Planar Solid Oxide Fuel Cells Via a Tape-Casting/Lamination/Co-Firing Technique," *J. Power Sources*, **195** [9] 2463-9 (2010).

<sup>19</sup>M. Rieu, P. K. Patro, T. Delahaye, and E. Bouyer, "Fabrication and Characterization of Anode-Supported BaIn<sub>0.3</sub>Ti<sub>0.7</sub>O<sub>2.85</sub> Thin Electrolyte for Solid Oxide Fuel Cell," *Int. J. Appl. Ceram. Technol.*, **9** [6] 1049-57 (2012).

<sup>20</sup>A. G. Evans and J. W. Hutchinson, "The Thermomechanical Integrity of Thin Films and Multilayers," *Acta Metall.*, **43** [7] 2507-30 (1995).

<sup>21</sup>P. Z. Cai, D. J. Green, and G. L. Messing, "Constrained Densification of Alumina/Zirconia Hybrid Laminates, I: Experimental Observations of Processing Defects," *J. Am. Ceram. Soc.*, **80** [8] 1929-39 (1997).

<sup>22</sup>ASTM Standard C373, 1988, *Standard Test Method for Water Absorption, Bulk Density, Apparent Porosity, and Apparent Specific Gravity of Fired White-ware Products*. ASTM-International, West Conshohocken, PA, 2006.

<sup>23</sup>ASTM Standard B106, *Standard Test Methods for Flexivity of Thermostat Metals*. ASTM-International, West Conshohocken, PA, 2008.

<sup>24</sup>C. Brugnoli, U. Ducati, and M. Scagliotti, "SOFC Cathode/Electrolyte Interface. Part I: Reactivity Between La<sub>0.85</sub>Sr<sub>0.15</sub>MnO<sub>3</sub> and ZrO<sub>2</sub>-Y<sub>2</sub>O<sub>3</sub>," *Solid State Ionics*, **76** [3-4] 177-82 (1995).

<sup>25</sup>S. Jiang, "Development of Lanthanum Strontium Manganite Perovskite Cathode Materials of Solid Oxide Fuel Cells: A Review," *J. Mater. Sci.*, **43** [21] 6799-833 (2008).

<sup>26</sup>C. Xia, W. Rauch, W. Wellborn, and M. Liu, "Functionally Graded Cathodes for Honeycomb Solid Oxide Fuel Cells," *Electrochem. Solid-State Lett.*, **5** [10] A217-20 (2002).

<sup>27</sup>V. Sprenkle, N. Canfield, D. Kerry, K. Meinhardt, and J. Stevenson, "Supporting electrodes for Solid Oxide Fuel Cells and other Electrochemical Devices"; US Patent Application US 2008/0038611 A1, 2008. 18.

<sup>28</sup>K. Wang, R. Ran, Y. Hao, Z. Shao, W. Jin, and N. Xu, "A High-Performance No-Chamber Fuel Cell Operated on Ethanol Flame," *J. Power Sources*, **177** [1] 33-9 (2008).

<sup>29</sup>J. L. Aguilar-Arias and D. Hotza, "Configuraciones Alternativas Para Celdas De Combustible De Óxido Sólido," *Rev. Latinoam. Metal. Mater.*, **33** [2] 172-85 (2012).

<sup>30</sup>D. R. Hardesty and F. J. Weinberg, "Burners Producing Large Excess Enthalpies," *Combust. Sci. Technol.*, **8** [5-6] 201-14 (1973).

<sup>31</sup>H. Kronmayer, D. Barzan, M. Horiuchi, S. Saganuma, Y. Tokutake, C. Schulz, and W. G. Bessler, "A Direct-Flame Solid Oxide Fuel Cell (DFFC) Operated on Methane, Propane, and Butane," *J. Power Sources*, **166** [1] 120-6 (2007).

<sup>32</sup>J. L. Aguilar-Arias, "Células a Combustível de Óxido Sólido Planares: Processamento e Avaliação do Desempenho Usando Álcool Como Combustível. (Planar Solid Oxide Fuel Cells: Processing and Performance Evaluation Using Alcohol as Fuel)"; Ph. D. Thesis, Graduate Program of Materials Science and Engineering., Federal University of Santa Catarina, Florianópolis, Brazil, 2012.

<sup>33</sup>S. P. Jiang and S. H. Chan, "A Review of Anode Materials Development in Solid Oxide Fuel Cells," *J. Mater. Sci.*, **9** [14] 4405-39 (2004).

<sup>34</sup>T. Hikita, "Research and Development of Planar Solid Oxide Fuel Cells at Tokyo Gas"; pp. 674-81 in *Science and Technology of Zirconia V*, Edited by S. P. Badwal, M. J. Bannister, and R. H. Hannik. Technomic Publishing Co., Lancaster, PA, 1993.

<sup>35</sup>NIST Technical Note 1297, *Guidelines for Evaluating and Expressing the Uncertainty of NIST Measurement Results*. National Institute of Standards and Technology, Gaithersburg, USA, 1994.

<sup>36</sup>K. K. Srivastava, R. N. Patil, C. B. Choudhary, K. V. Gokhale, and E. C. Subba-Rao, "Revised Phase Diagram of the System ZrO<sub>2</sub>-YO<sub>1.5</sub>," *Trans. Brit. Ceram. Soc.*, **73** [5] 85-91 (1974).

<sup>37</sup>L. L. Sun, Y. Hao, C. M. Zhang, R. Ran, and Z. P. Shao, "Coking-Free Direct-Methanol-Flame Fuel Cell with Traditional Nickel-Cermet Anode," *Int. J. Hydrogen Energy*, **35** [15] 7971-81 (2010). □